south of G25.5+0.0, coincides with the center of gravity of the VHE emission and is therefore the most promising counterpart candidate. This still unidentified source was also serendipitously detected by the BeppoSAX x-ray satellite instrument and also in the hard x-ray (20 to 100 keV) band in the galactic plane survey performed with the Integral (International Gamma-Ray Astrophysics Laboratory) satellite (*25*).

For the two remaining sources, HESS J1813-178 and HESS J1614-518, no plausible counterparts have been found at other wavelengths. HESS J1813-178 is not spatially coincident with any counterparts in the region but lies 10 arc min from the center of the radio source W 33. W 33 extends over 15 arc min, with a compact radio core (G12.8-0.2) that is 1 arc min across (*26*). The region is highly obscured and has indications of recent star formation (*27*). In its extended emission and location close to an association of hot O and B stars, HESS J1813-178 resembles the unidentified TeV source discovered by HEGRA, TeV J2032+4130 (*28*), and the first HESS unidentified γ-ray source, HESS J1303-63 (*29*). HESS J1614-518 has no plausible SNR or pulsar counterpart. This source is in the field of view of HESS J1616-508, which is located nearby (~1° away). The lack of any counterparts for these two sources suggests the exciting possibility of a new class of "dark" particle accelerators in the Galaxy.

In conclusion, we have on the basis of the survey generated an unbiased catalog of VHE γ-ray sources in the central region of our Galaxy, extending our multiwavelength knowledge of the Milky Way into the VHE domain. Three of the eight newly discovered sources are potentially associated with SNRs, two with EGRET sources. In three cases an association with pulsar-powered nebulae is not excluded. At least two sources have no identified counterpart in radio or x-rays, which suggests the exciting possibility of a new class of "dark" nucleonic particle accelerators. This catalog provides insights into particle acceleration in our Galaxy and adds a piece to the long-standing puzzle of cosmic-ray origin.

References and Notes

1. R. Atkins *et al.*, *Astrophys. J.* **608**, 680 (2004).
2. M. Amenomori *et al.*, *Astrophys. J.* **580**, 887 (2002).
3. A. Daum *et al.*, *Astropart. Phys.* **8**, 1 (1997).
4. F. Aharonian *et al.*, *Astron. Astrophys.* **395**, 803 (2002).
5. W. Benbow *et al.*, in *International Symposium on High-Energy Gamma-Ray Astronomy*, F. A. Aharonian, H. J. Völk, D. Horns, Eds. (AIP Conference Proceedings 745, 2005), pp. 611–616.
6. K. Bernlöhr *et al.*, *Astropart. Phys.* **20**, 111 (2003).
7. P. Vincent *et al.*, in *Proceedings of the 28th International Cosmic Ray Conference*, T. Kajita *et al.*, Eds. (Universal Academy Press, Tokyo, 2003), pp. 2887–2890.
8. S. Funk *et al.*, *Astropart. Phys.* **22**, 285 (2004).
9. F. Aharonian *et al.*, *Astropart. Phys.* **6**, 369 (1997).
10. F. Aharonian *et al.*, *Astron. Astrophys.* **425**, L13 (2004).
11. F. Aharonian *et al.*, *Nature* **432**, 75 (2004).
12. F. Aharonian *et al.*, *Astron. Astrophys.* **430**, 865 (2005).
13. D. A. Green, *Bull. Astron. Soc. India* **32**, 335 (2004).
14. R. N. Manchester, G. B. Hobbs, A. Teoh, M. Hobbs, *Astron. J.*, in press (available at http://xxx.lanl.gov/abs/astro-ph/0412641).
15. R. C. Hartman *et al.*, *Astrophys. J. Suppl. Ser.* **123**, 79 (1999).
16. N. E. Kassim, *Astron. J.* **103**, 943 (1992).
17. L. Blitz, M. Fich, A. A. Stark, *Astrophys. J. Suppl. Ser.* **49**, 183 (1982).
18. N. E. Kassim, *Nature* **343**, 146 (1990).
19. P. L. Nolan, W. F. Tompkins, I. A. Grenier, P. F. Michelson, *Astrophys. J.* **597**, 615 (2003).
20. B. M. Gaensler, N. S. Schulz, V. M. Kaspi, M. J. Pivovaroff, W. E. Becker, *Astrophys. J.* **588**, 441 (2003).
21. K. Torii *et al.*, *Astrophys. J.* **494**, L207 (1998).
22. E. V. Gotthelf, R. Petre, U. Hwang, *Astrophys. J.* **487**, L175 (1997).
23. J. Vink, *Astrophys. J.* **604**, 693 (2004).
24. A. Bamba, M. Ueno, K. Koyama, S. Yamauchi, *Astrophys. J.* **589**, 253 (2003).
25. A. Malizia *et al.*, in *Proceedings of the V INTEGRAL Workshop*, Munich, 16 to 20 February 2004 (available at http://xxx.lanl.gov/abs/astro-ph/0404596).
26. A. Haschick, P. T. P. Ho, *Astrophys. J.* **267**, 638 (1983).
27. E. Churchwell, *Astron. Astrophys. Rev.* **2**, 79 (1990).
28. F. Aharonian *et al.*, *Astron. Astrophys.* **393**, L37 (2002).
29. M. Beilicke *et al.*, in *International Symposium on High-Energy Gamma-Ray Astronomy*, F. A. Aharonian, H. J. Völk, D. Horns, Eds. (AIP Conference Proceedings 745, 2005), pp. 347–352.
30. T. Li, Y. Ma, *Astrophys. J.* **272**, 317 (1983).
31. M. de Naurois *et al.*, in *Proceedings of the 28th International Cosmic Ray Conference*, T. Kajita *et al.*, Eds. (Universal Academy Press, Tokyo, 2003), pp. 2907–2910.

32. The support of the Namibian authorities and of the University of Namibia in facilitating the construction and operation of HESS is gratefully acknowledged, as is the support of the German Ministry for Education and Research (BMBF), the Max Planck Society, the French Ministry for Research, the CNRS-IN2P3 and the Astroparticle Interdisciplinary Programme of the CNRS, the UK Particle Physics and Astronomy Research Council (PPARC), the Institute of Particle and Nuclear Physics of the Charles University, the South African Department of Science and Technology and National Research Foundation, and the University of Namibia. We appreciate the excellent work of the technical support staff in Berlin, Durham, Hamburg, Heidelberg, Palaiseau, Paris, Saclay, and Namibia in the construction and operation of the equipment. L.C., C.M., M.O., I.R., and M.T. are also affiliated with the European Associated Laboratory for Gamma-Ray Astronomy, jointly supported by CNRS and the Max Planck Society.

13 December 2004; accepted 18 January 2005
10.1126/science.1108643

Chemical Detection with a Single-Walled Carbon Nanotube Capacitor

E. S. Snow,* F. K. Perkins, E. J. Houser, S. C. Badescu, T. L. Reinecke

We show that the capacitance of single-walled carbon nanotubes (SWNTs) is highly sensitive to a broad class of chemical vapors and that this transduction mechanism can form the basis for a fast, low-power sorption-based chemical sensor. In the presence of a dilute chemical vapor, molecular adsorbates are polarized by the fringing electric fields radiating from the surface of a SWNT electrode, which causes an increase in its capacitance. We use this effect to construct a high-performance chemical sensor by thinly coating the SWNTs with chemoselective materials that provide a large, class-specific gain to the capacitance response. Such SWNT chemicapacitors are fast, highly sensitive, and completely reversible.

Sorption-based microsensors are currently a leading candidate for low-power, compact chemical vapor detection for defense, homeland security, and environmental-monitoring applications (*1*–*9*). Such sensors combine a nonselective transducer with chemoselective materials that serve as a vapor concentrator, resulting in a highly sensitive detector that responds selectively to a particular class of chemical vapor. An array of such sensors, each coated with a different chemoselective material, produces a response fingerprint that can detect and identify an analyte (*1*–*3*). Sorption-based sensors provide sensitive detection for vapors ranging from volatile organic compounds to semivolatile chemical nerve agents, although low–vapor pressure materials such as explosives are challenging because they do not produce a sufficiently high concentration of vapor (*4*).

The transducer elements for such sensor arrays need to be small, low-power, and compatible with conventional microprocessing technology. Among the choice of transducers are mechanical oscillators that respond to changes in mass (*1*, *2*), chemicapacitors that detect changes in dielectric properties (*4*–*6*), and chemiresistors that monitor the resistance of a polymer laced with conductive particles (*7*–*9*). Of these transducers, chemicapacitors (*4*) and chemiresistors (*7*, *8*) are the best suited for low-power sensor arrays. Chemiresistors are simple to implement, but instability of the con-

Naval Research Laboratory, Washington, DC 20375, USA.

*To whom correspondence should be addressed. E-mail: snow@bloch.nrl.navy.mil

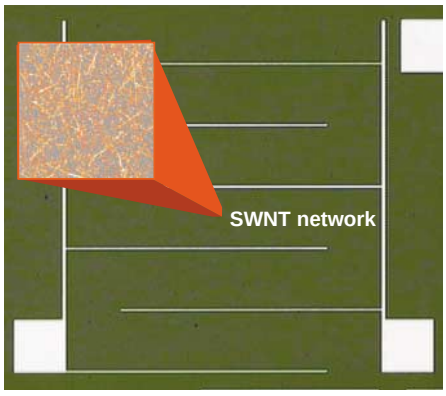

Fig. 1. Optical micrograph of a SWNT chemicapacitor. The region between the electrodes is covered with an optically transparent but electrically continuous network of SWNTs (shown in the inset atomic force microscope image). The capacitance was measured by applying an ac bias between this top surface and the underlying conducting Si substrate. The electrodes were interdigitated to allow simultaneous measurement of the network resistance, but were electrically shorted for data collected here.

Table 1. Capacitance response to various chemical vapors. Listed are the measured values of $\Delta C/C$ corresponding to P/P_0 = 1%. Also listed are the values of the dipole moment, μ, the equilibrium vapor pressure, P_0, at 25°C, and the vapor concentration, P, in parts per million.

Chemical vapor	P_0 (mbar) at 25°C	P (ppm) at 1% P/P_0	μ (D)	$\Delta C/C \times 10^{-3}$ at 1% P/P_0
Benzene	127	1290	0	0.3 ± 0.1
Hexane	200	2030	0	0.4
Heptane	61	618	0	0.2
Toluene	38	385	0.38	0.5
Trichloroethylene	91	922	0.8	0.6
Chloroform	257	2600	1.04	0.8
Trichloroethane	38	385	1.4	0.8
Isopropyl alcohol	108	1093	1.58	3.8
Ethanol	78	792	1.69	3.0
Chlorobenzene	16	162	1.69	0.4
Methyl alcohol	168	1702	1.7	2.7
Tetrahydrofuran	215	2180	1.75	5.9
Ethyl acetate	127	1290	1.78	3.1
Water	32	324	1.85	0.5
Dichlorobenzene	2	20.3	2.5	0.4
Acetone	304	3080	2.88	6.1
Dimethylmethylphosphonate	1.6	16.2	3.62	10.2
N,*N*-dimethylformamide	5	50.7	3.82	9.3
Dinitrotoluene	0.0028	0.028	4.39	0.5

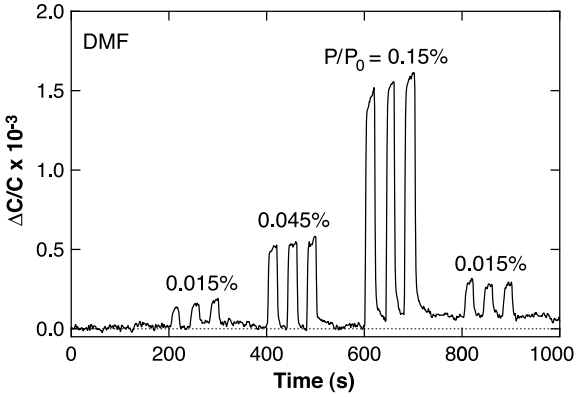

Fig. 2. Measured relative capacitance change, $\Delta C/C$, of a SWNT chemicapacitor in response to repeated 20-s doses of dimethyl formamide (DMF) at varying concentrations noted in the figure.

ductive particle/polymer interface can be a disadvantage. Chemicapacitors are more stable but can take minutes to respond and recover (*4*). This slow response is limited by the time necessary to load and then remove the analyte from the relatively thick layers of chemoselective dielectric (~1 μm) that are typically used.

We describe a chemicapacitor constructed from single-walled carbon nanotube (SWNT) electrodes that combines the features of stability, high sensitivity to a broad range of analytes, and fast response time. The capacitance response of the SWNT chemicapacitor is dominated by surface adsorbates, which allows us to use very thin layers of chemoselective material down to, and including, a single molecular monolayer. By achieving chemical selectivity with such a monolayer, we eliminate the time required to load and refresh a thick, chemoselective dielectric and can perform sensitive, real-time sensing.

The surface capacitance effect is caused by the large electric-field gradient radiating from the ~1-nm-diameter SWNT electrodes. This transduction mechanism is quite general and can be used to detect both volatile organics and low–vapor pressure explosives. We demonstrate the compatibility of this transducer with conventional chemoselective polymers by using a hydrogen-bonding polymer to achieve a minimum detectable level (MDL) of 0.5 parts per billion (ppb) for dimethylmethylphosphonate (DMMP), a simulant for the chemical nerve agent sarin.

To improve the response time, we replaced the polymer layer with a hydrogen-bonding molecular monolayer. In this case, we achieve a MDL of 50 ppb for DMMP with a 90% recovery time, t_{90}, < 4 s. By combining 1-nm-diameter electrodes with molecular-scale functionalization, we achieve a sorption-based chemicapacitor that offers stability, real-time sensing, and a high sensitivity to a wide spectrum of chemical vapors ranging from volatile organics to low–vapor pressure explosives.

We fabricated the SWNT chemicapacitors by using chemical vapor deposition to grow a SWNT network on a 250-nm-thick thermal oxide on a degeneratively doped silicon substrate (*10*). For each sensor, a 2 mm by 2 mm interdigitated array of Pd electrodes was deposited on top of the SWNT network by using photolithography and lift-off. The interdigitated electrodes provide contacts for the simultaneous measurement of both the capacitance and the resistance of the SWNT network. The region inside the array was protected by photoresist, and the unprotected SWNTs were removed from the substrate by a CO_2 snowjet. The photoresist was then removed, which left the SWNT network exposed to the ambient environment. We prepared the chemical vapors by mixing saturated vapors of the analyte with dry air at 25°C.

The SWNT network forms an array of nanoscale electrodes that serves as one plate of the capacitor, with the other electrode formed by the heavily doped Si substrate (Fig. 1). We measured the capacitance by applying a 30-kHz, 0.1-V ac voltage between the SWNTs and the substrate and detecting the out-of-phase ac current with a lock-in amplifier. The measured capacitance, ~ 10 nF/cm^2, is close to the parallel-plate value corresponding to a 250-nm-thick SiO_2 gate dielectric and is the expected value for an inter-SWNT spacing less than the SiO_2 thickness (*11*).

Under an applied bias, fringing electric fields (~10^5 to 10^6 V/cm, for a 0.1-V bias) radiate outward from the SWNTs. These fringing fields are strongest at the SWNT surface and produce a net polarization of the adsorbates that we detect as an increase in capacitance. The relative capacitance change, $\Delta C/C$, of one such device in response to repeated 20-s doses of *N*,*N*-dimethylformamide (DMF) at varying vapor concentrations (Fig. 2) shows that the observed response is rapid (limited by the 4-s response time of our vapor-delivery system), proportional

to the analyte concentration, and completely reversible. Of the chemical vapors that we have tested (Table 1), we observe a similar, rapid capacitance response that is completely reversible upon removal of the vapor. We also note that ΔC is independent of the applied voltage for $V_{ac} < 1$ V, which indicates that the polarization is a linear function of the electric field.

In Table 1, we list values of $\Delta C/C$ for a number of chemical vapors, each measured at a fixed fraction, $P/P_0 = 1\%$, of the equilibrium vapor pressure P_0. We also list literature values of P_0 (*12*), the vapor concentration, P, in parts per million (ppm) at $P/P_0 = 1\%$, and the molecular dipole moment, μ (*12*, *13*). In Fig. 3, we plot the values of $\Delta C/C$ reported in Table 1 for each of the analytes versus their respective dipole moments.

In Fig. 3, we observe that for several analytes, the magnitude of the capacitance response correlates with the value of its dipole moment. Nonpolar molecules such as hexane and benzene produce a small response, whereas relatively polar molecules like DMMP and DMF produce a large capacitance response. This correlation with dipole moment holds under the condition that the vapors are each delivered at a constant value of P/P_0, and not for a constant value of P. For example, acetone ($\mu = 2.88$ D) and DMMP ($\mu = 3.62$ D) produce a comparable capacitance response when both are delivered at $P/P_0 = 1\%$ even though this condition corresponds to vapor concentrations of 3080 ppm and 16 ppm, respectively. Several analytes such as chlorobenzene, 1,2-dichlorobenzene, 2,4-dinitrotoluene, and water (represented by squares in Fig. 3) produce a small capacitance response even though they have a relatively large dipole moment. These data indicate that the magnitude of the capacitance response is strongly modified by surface interactions.

The polarizability of a free vapor molecule is given by $\gamma = \gamma_{mol} + \frac{\mu^2}{3kT}$ (*14*), where the first term arises from the intrinsic molecular polarizability, γ_{mol}, and the second term arises from the field-induced alignment of the otherwise randomly oriented molecular dipole moment. From the Clausius-Mossotti equation, this polarizability is related to the dielectric constant, ε, by

$$\varepsilon = 1 + 4\pi\frac{N\gamma}{1 - \frac{4\pi}{3}N\gamma},$$

where N is the number of molecules, which is proportional to the vapor pressure, P. Thus, for a dilute vapor, the capacitance response should scale as $P\mu^2$. Instead, we observe that $\Delta C/C \propto \frac{P}{P_0}$ and that there are large deviations from simple μ^2 behavior.

For surface adsorbates, the polarization will be proportional to the number of the adsorbates, which is proportional to $\frac{P}{P_0}e^{(E_b - E_i)/kT}$ (*15*), where E_i is the analyte mutual interaction energy and E_b is the binding energy to the SWNT surface (approximately the thermal energy, kT, for physisorbed molecules). Thus, for adsorbates, we expect the capacitance to scale as P/P_0 with significant analyte-to-analyte variations caused by the differences in binding and interaction energies.

Additionally, surface interactions will preferentially orient the molecular dipole moment. For example, the low response of chlorobenzene, 1,2-dichlorobenzene, and 2,4-dinitrotoluene can be understood in the context of surface interactions. These analytes indicate that the capacitance response scales with the component of the dipole moment oriented perpendicular to the SWNT surface. Each of these molecules has a dipole moment that is oriented in the plane of an aromatic ring. Our density functional calculations (*16*) indicate that the lowest energy configuration corresponds to the ring lying flat on the SWNT surface. In this orientation, the dipole moment lies perpendicular to the radial electric field, which minimizes the polarization and results in a small capacitance effect. The cause of the small water response is not clear. However, it has been suggested that the dipole moment of water also aligns tangentially to the SWNT surface in its lowest energy configuration (*17*).

Our initial density functional calculations (*16*) indicate that for some analytes such as acetone the primary polarization effect derives from the field dependence of the binding energy, which causes a change in the number of adsorbates by a factor $\sim\Delta E_b/kT$. However, further study is needed to understand the precise polarization mechanism, which will differ for different analytes.

The rapid, completely reversible capacitance response that we observe contrasts with the behavior of SWNT chemiresistors (*18*–*25*). SWNT chemiresistors respond to a narrower range of analytes, and typically the resistance recovers very slowly after exposure. Part of the reason for this difference is that the SWNT chemiresistors detect charge transfer from analytes, whereas the SWNT chemicapacitors operate via a different transduction mechanism, the polarization of surface adsorbates (*26*). Our experience measuring both effects simultaneously on the same device indicates that, for most vapors, the capacitance response is more sensitive, recovers much faster, and applies to a broader range of analytes (*27*).

Because most chemical vapors, ranging from volatile organics such as acetone to low–vapor pressure solids such as 2,4-dinitrotoluene, produce an easily measured capacitance response, this transduction mechanism can be used to detect a broad spectrum of molecular analytes. To explore this possibility, we coated our sensors with a chemoselective polymer, HC,

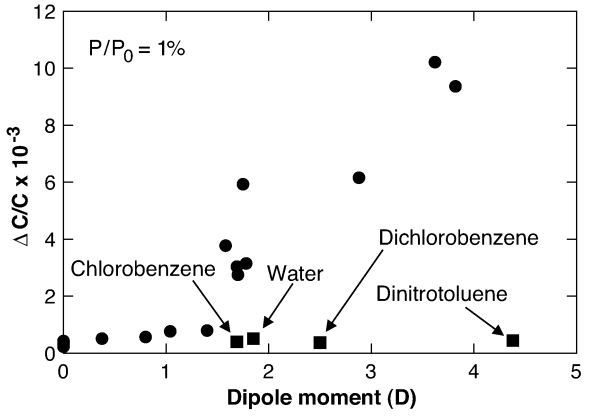

Fig. 3. Measured capacitance response to $P/P_0 = 1\%$ doses of various chemical vapors plotted as a function of their molecular dipole moment. The capacitance response generally increases with dipole moment; however, large deviations from this trend are observed.

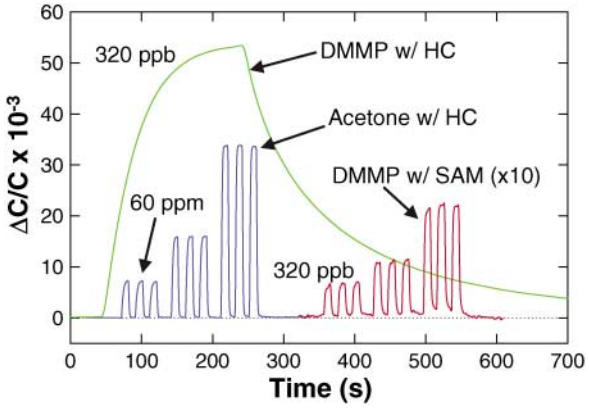

Fig. 4. Blue curve: Response to 10-s doses of acetone of a SWNT chemicapacitor coated with the polymer, HC. The concentration was set at 60, 180, and 540 ppm. Green curve: Response of the same HC-coated sensor to a single, 200-s dose of DMMP. Note the increased response time caused by the slower diffusion of the DMMP. Red curve: Response ($\times 10$) of a SAM-coated sensor to 10-s doses of DMMP. The concentration was set at 320 ppb, 960 ppb, and 2.9 ppm. Note the improvement in response time relative to the HC-coated sensor.

that we designed for preferential absorption of chemical nerve agents. HC is an acidic, strong–hydrogen-bonding polycarbosilane (*25*). We coated a sensor with a thin layer (~100 nm) of HC and tested the response to several analytes. The response of this polymer-coated sensor to repeated 10-s doses of acetone ranging from 60 to 540 ppm is shown in Fig. 4. The acetone produces a large, rapid response that is ~100 times larger than the response measured in the same sensor before the HC deposition. The HC concentrates the acetone vapor in the vicinity of the SWNTs, which increases the response while maintaining a rapid response time. The response to a single 200-s dose of DMMP delivered at 320 ppb shows that the measured gain for DMMP relative to the uncoated sensor is about 500 (Fig. 4). Note that the low diffusion rate of DMMP in the HC causes a slower recovery rate, t_{90} = 370 s. For water and chloroform, the polymer coating produces much lower response gains of 1 and 10, respectively. Thus, the HC provides a large chemically selective gain, demonstrating the feasibility of SWNT sorption-based chemical sensing.

These sensor characteristics compare favorably with those of commercial chemicapacitors. Using a signal-to-noise ratio of 3:1 as a detection criterion, we estimate that MDL = 0.5 ppm and $t_{90} < 4$ s for acetone and MDL = 0.5 ppb and t_{90} = 370 s for DMMP. For these same analytes, the commercial sensor achieves a MDL = 2 ppm and t_{90} = 228 s for acetone and MDL = 2 ppb and t_{90} = 3084 s for DMMP (*4*). We attribute our faster response and recovery times to the use of a much thinner layer of chemoselective material. For HC, the minimum layer thickness was limited by the tendency of the HC to form a discontinuous film below ~100 nm.

Our initial polymer-coated SWNT sensors achieve both higher sensitivity and faster response times than do current chemicapacitors. However, both of these properties can be substantially improved with a few design modifications. The sensitivity is currently limited by the small series capacitance of the thick SiO_2 layer. By thinning the SiO_2 layer or replacing it with a high–dielectric constant insulator (*28*), we estimate that we can increase the series capacitance by about a factor of 10, which should produce a comparable increase in response.

The response time for analytes such as DMMP is limited by diffusion through the layer of HC. Because the SWNT capacitor is based on a surface effect, we can improve the response time and still achieve chemical gain by using extremely thin layers of chemoselective material down to, and including, a single molecular monolayer.

To explore this limit of a chemoselective monolayer, we coated the SiO_2 surface with a self-assembled monolayer (SAM) of allyltrichlorosilane. We then reacted the terminal alkenes with hexafluoroacetone to produce a monolayer of hexafluoroisopropanol that partially covers the SWNTs with fluoroalchohol groups. The response of this SAM-coated sensor to repeated 10-s doses of DMMP ranging from 320 ppb to 2.9 ppm is shown in Fig. 4. For this sensor, the response tracks our vapor-delivery system, indicating that $t_{90} <$ 4 s, and we measured a MDL = 50 ppb. Notably, with the SAM coating, the capacitance response of DMMP relative to that of water is increased by a factor of 40, indicating that we achieved substantial chemically selective gain. These initial promising results indicate that optimization of the chemoselective monolayers to better cover the SWNTs, combined with improved sensor design, can result in a new class of sorption-based sensors that combine the features of low power, high sensitivity, and fast response time.

References and Notes

1. R. A. McGill *et al.*, *Sens. Actuators B* **65**, 10 (2000).
2. J. W. Grate, B. M. Wise, M. H. Abraham, *Anal. Chem.* **71**, 4544 (1999).
3. H. T. Nagle, S. S. Schiffman, R. Gutierrez-Osuna, *IEEE Spectr.* **35**, 22 (1998).
4. S. V. Patel *et al.*, *Sens. Actuators B* **96**, 541 (2003).
5. G. Delapierre, H. Grange, B. Chambaz, L. Destannes, *Sens. Actuators* **4**, 97 (1983).
6. A. Hierlemann *et al.*, *Sens. Actuators B* **70**, 2 (2000).
7. M. P. Eastman *et al.*, *J. Electrochem. Soc.* **146**, 3907 (1999).
8. M. C. Lonergan *et al.*, *Chem. Mater.* **8**, 2298 (1996).
9. J. R. Li, J. R. Xu, M. Q. Zhang, M. Z. Rong, *Carbon* **41**, 2353 (2003).
10. E. S. Snow, J. P. Novak, P. M. Campbell, D. Park, *Appl. Phys. Lett.* **82**, 2145 (2003).
11. E. S. Snow, P. M. Campbell, J. P. Novak, *Appl. Phys. Lett.* **86**, 033105 (2005).
12. D. R. Lide, *CRC Handbook of Chemistry and Physics* (CRC Press, Boca Raton, FL, ed. 75, 1995), pp. 15-43–15-49.
13. G. M. Kosolapoff, *J. Chem. Soc.* 3222 (1954).
14. J. D. Jackson, *Classical Electrodynamics* (Wiley, New York, ed. 2, 1975), pp. 155–158.
15. S. Brunauer, P. H. Emmett, E. Teller, *J. Am. Chem. Soc.* **60**, 309 (1938).
16. Density functional calculations of adsorbates on graphene sheets in uniform electric fields were performed using the generalized-gradient approximation and the Perdue, Burke, Ernzerhof parameterization of exchange and correlation in the Gaussian 03 localized-basis package (Gaussian 03, Revision C.02; M. J. Frisch *et al.*, Gaussian, Inc., Pittsburgh PA, 2003).
17. J. H. Walther, R. Jaffe, T. Halicioglu, P. Koumoutsakos, *J. Phys. Chem. B* **105**, 9980 (2001).
18. J. Kong *et al.*, *Science* **87**, 622 (2000).
19. L. Valentini *et al.*, *Appl. Phys. Lett.* **82**, 961 (2003).
20. T. Someya, J. Small, P. Kim, C. Nuckolls, J. T. Yardley, *Nano Lett.* **3**, 877 (2003).
21. J. Li *et al.*, *Nano Lett.* **3**, 929 (2003).
22. A. Goldoni, R. Larciprete, L. Petaccia, S. Lizzit, *J. Am. Chem. Soc.* **125**, 11329 (2003).
23. P. Qi *et al.*, *Nano Lett.* **3**, 347 (2003).
24. L. Valentini *et al.*, *Diamond Relat. Mater.* **13**, 1301 (2004).
25. J. P. Novak *et al.*, *Appl. Phys. Lett.* **83**, 4026 (2003).
26. Charge transfer from an analyte can potentially cause a capacitance response by changing the quantum capacitance of the nanotubes. We have simulated this chemical doping effect by applying to the substrate a small dc offset to the ac bias, which increases the charge in the SWNTs. By measuring the resulting capacitance and resistance responses, we calibrated the effect of a charge offset. For the vapors we have tested, most do not produce a measurable resistance response, and those that do, produce a resistance change that is much too small (based on this calibration) to account for the change in capacitance.
27. For an example, see the supplementary data available at *Science* Online.
28. B. M. Kim *et al.*, *Appl. Phys. Lett.* **84**, 1946 (2004).

29. We gratefully acknowledge financial support from the Homeland Security Advanced Research Projects Administration, the Office of Naval Research, and the Naval Research Laboratory Nanoscience Institute.

Supporting Online Material

www.sciencemag.org/cgi/content/full/307/5717/1942/DC1
SOM Text
Fig. S1

27 December 2004; accepted 1 February 2005
10.1126/science.1109128

Light Scattering to Determine the Relative Phase of Two Bose-Einstein Condensates

M. Saba,* T. A. Pasquini, C. Sanner, Y. Shin, W. Ketterle, D. E. Pritchard

We demonstrated an experimental technique based on stimulated light scattering to continuously sample the relative phase of two spatially separated Bose-Einstein condensates of atoms. The phase measurement process created a relative phase between two condensates with no initial phase relation, read out the phase, and monitored the phase evolution. This technique was used to realize interferometry between two trapped Bose-Einstein condensates without need for splitting or recombining the atom cloud.

The outstanding property of atoms in a Bose-Einstein condensate (BEC) is their coherence: They all have the same phase. This property became apparent when high-contrast interference between condensates was observed (*1–3*). Phase coherence between spatially separated condensates has led to the observation of a host of phenomena, including Josephson oscillations (*3*, *4*), number squeezing (*5*), and the transition from superfluid to Mott insulator (*6*).

The evolution of the phase is affected by external potentials acting on the atoms and has